Blind Deblurring of THz Time-Domain Images Based on Low-Rank Representation

Marina Ljubenović[1][a], Mário A. T. Figueiredo[2][b] and Arianna Traviglia[1][c]

[1]*Center for Cultural Heritage Technology, Istituto Italiano di Tecnologia, Venice, Italy*
[2]*Instituto de Telecomunicações, Instituto Superior Técnico, Lisbon, Portugal*

Keywords: THz TDS, Deblurring, Denoising, Low-Rank.

Abstract: Terahertz (THz) time-domain imaging holds immense potential for material characterization, capturing three-dimensional data across spatial and temporal dimensions. Despite its capabilities, the technology faces hurdles such as frequency-dependent beam-shape effects and noise. This paper proposes a novel, dual-stage framework for improving THz image resolution beyond the wavelength limit. Our method combats blur at lower frequencies and noise at higher frequencies. The first stage entails selective deblurring of lower-frequency bands, addressing beam-related blurring, while the second stage involves denoising the entire THz hyperspectral cube through dimensionality reduction, exploiting its low-rank structure. The synergy of these advanced techniques—beam shaping, noise removal, and low-rank representation—forms a comprehensive approach to enhance THz time-domain images. We present promising preliminary results, showcasing significant improvements across all frequency bands, which is crucial as samples may display varying features across the THz spectrum. Our ongoing work is extending this methodology to complex scenarios such as analyzing multilayered structures in closed ancient manuscripts. This approach paves the way for broader application and refinement of THz imaging in diverse research fields.

1 INTRODUCTION

Terahertz (THz) radiation occupies a region between the microwave and infrared portions of the electromagnetic spectrum, approximately spanning from 0.1 to 10 THz. This radiation can penetrate various non-conducting materials, which makes it suitable for imaging diverse objects. THz waves have longer wavelengths than visible and infrared light, which traditionally limits their spatial resolution due to diffraction. The advent of THz time-domain imaging has marked a significant milestone in the field of spectroscopy and imaging, offering unparalleled non-destructive analysis and resolution capabilities in a diverse array of applications ranging from security screening and biomedical imaging to cultural heritage (Kemp et al., 2003; Darmo et al., 2004; Fukunaga, 2012). The unique interaction of THz radiation with different materials allows for the extraction of material-specific signatures, which are imperative for

accurate imaging and analysis (Hashimoto and Tripathi, 2022).

In time-domain THz imaging in the reflection geometry, short pulses of THz radiation are directed onto an object. Some of the radiation is reflected, transmitted, or scattered depending on the object's properties. A detector measures the time delay and intensity of the returning pulses, creating a time-resolved profile of the radiation, often referred to as a waveform, for each pixel of the image. The structure of a THz time-domain image is inherently three-dimensional (3D), with two spatial dimensions and one temporal dimension (x, y, t). For each pixel (x, y), there is a corresponding time-domain waveform (t) that contains information about the THz signal's interaction with the object at that point. This waveform can provide a wealth of information, including phase and amplitude data that are sensitive to the material's characteristics such as thickness, density, and chemical composition. In the frequency domain, THz time-domain images have the shape of 3D hyperspectral (HS) cubes where each band corresponds to different frequencies.

However, despite its considerable potential, the

---

practical deployment of THz imaging, particularly in the 0.35–6 THz range, has been challenged by a variety of factors, including frequency-dependent beam-shape effects and the inherent noise present in these images (Ljubenović et al., 2020). Additionally, the resolution, being wavelength-dependent, is constrained by the THz wavelength, which typically prevents resolving features smaller than the wavelength itself. Figure 1 illustrates beam shape and noise effects on different bands of THz time-domain images.

1.1 Related Work

In reflection geometry, the shape of the THz beam plays a pivotal role in the quality of the acquired images. The spatial distribution of the beam, which can be significantly affected by diffraction and scattering, often leads to images with less than optimal resolution. To circumvent these limitations, advanced methodologies have been developed to manipulate and refine the beam profile, leading to improved image resolution and contrast (Recur et al., 2012; Podzorov et al., 2010; Popescu and Hellicar, 2010). Nevertheless, these methods are mostly focused on single-frequency THz images and noiseless scenarios.

In recent times, there has been an emergence of methods leveraging neural networks for the restoration of THz images, including super-resolution (Li et al., 2017; Long et al., 2019), deblurring (Ljubenović et al., 2020), and noise reduction (Dutta et al., 2022). However, these techniques often rely on synthetic datasets for training due to the scarcity of real-world training samples. Consequently, while they exhibit promise, their performance tends to be limited when applied to real THz image data. Noise removal techniques are of paramount importance, as THz time-domain images are particularly susceptible to noise stemming from a variety of sources including environmental conditions and system-induced artefacts.

HS data is naturally low-rank because the spectral bands often have a high correlation; only a few distinct materials are present in the scene, which reflect similar spectral signatures (Nascimento and Bioucas-Dias, 2007). The idea is that while the dataset is high-dimensional, the intrinsic dimensionality—due to redundancies and correlations in the spectral domain—is much lower. For denoising, the low-rank property has been exploited by assuming that the clean HS image data resides in a low-dimensional subspace. Techniques such as robust principal component analysis (RPCA) and its variants can separate the low-rank clean image from sparse noise (Candès et al., 2011). These methods assume that the noise

is sparse and uncorrelated, allowing it to be separated from the low-rank data matrix. Several methods by Zhuang *et al.* are based on a similar assumption providing state-of-the-art results for denoising remote sensing HS data (Zhuang and Bioucas-Dias, 2018; Zhuang et al., 2021). Additionally, some of these methods exploit a plug-and-play framework where the core idea is to decouple the inversion process (i.e., restoration) from the denoising process (Venkatakrishnan et al., 2013).

Furthermore, image restoration techniques based on low-rank representation have emerged as a powerful tool to exceed the diffraction limit imposed by the THz wavelength (Ljubenović et al., 2022). These techniques exploit the inherent sparsity of the image data in the THz spectral range, enabling the reconstruction of high-resolution and sharp images from low-resolution counterparts. By disentangling the true signal from the noise, low-rank representation methods provide a robust framework for the restoration of THz time-domain images without the need for hardware improvements.

In this paper, we aim to integrate these advanced techniques—beam shaping in reflection geometry, noise removal, low-rank representation, and plug-and-play-based restoration—to present a comprehensive framework that pushes the boundaries of THz time-domain imaging. Our approach leverages the synergies between these methods, fostering developments that could improve the quality and applicability of THz imaging across multiple disciplines.

2 PROPOSED METHOD

We observed that bands associated with lower frequencies exhibit stronger blur due to the larger beam waist sizes at these frequencies. To address this issue, our approach involves a sequential two-step method: initially, we apply a targeted deblurring process to the lower-frequency bands. Subsequently, we perform denoising of the entire THz HS cube by applying dimensionality reduction and a plug-and-play approach, taking advantage of its inherent low-rank structure.

The rationale underpinning our proposed method is based on the insight that dimensionality reduction applied to the original data cube tends to retain certain blurring artifacts within the subspace components (as seen in Figure 2). Conversely, when this reduction is carried out on data that has already been deblurred, there is a notable preservation of finer details (as illustrated in Figure 3).

Assuming additive noise, an observation model for THz HS image with b spectral bands where each
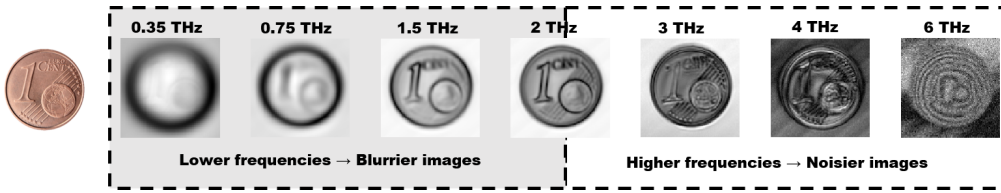
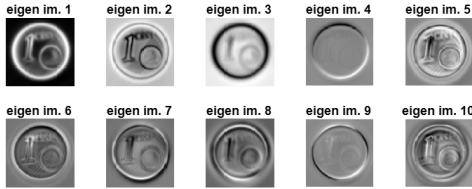Figure 1: Bands corresponding to lower, medium, and higher frequencies.

Figure 2: Subspace components when dimensionality reduction is performed on the original data cube.
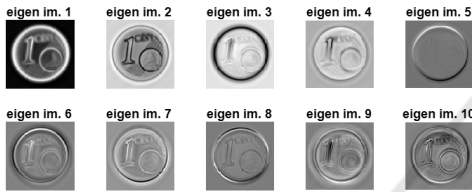

Figure 3: Subspace components when dimensionality reduction is performed after deblurring.

band has n pixels is

$$\mathbf{Y} = \mathbf{H}\mathbf{X} + \mathbf{N}, \quad (1)$$

where $\mathbf{Y} \in \mathbb{R}^{b \times n}$ and $\mathbf{X} \in \mathbb{R}^{b \times n}$ represent an observed (blurred and noisy) and underlying (clean) THz HS image respectively, and $\mathbf{N} \in \mathbb{R}^{b \times n}$ stands for Gaussian i.i.d. noise. The matrix $\mathbf{H} = \text{bkdiag}(\mathbf{H}_1, \mathbf{H}_2, ..., \mathbf{H}_b) \in \mathbb{R}^{bn \times bn}$, representing the unknown blurring degradation, is a block diagonal matrix, where each block corresponds to a 2D cyclic convolution related to the point spread function (PSF) of the corresponding band.

2.1 Band-by-Band Deblurring

We propose deblurring each separate band up to some (predefined) frequency limit. The vectorised observed and underlying images corresponding to each band are related through the observation model:

$$\mathbf{y}_i = \mathbf{H}_i \mathbf{x}_i + \mathbf{n}_i, \quad (2)$$

with $i = 1, 2, ..., m$, and $m < b$. Here, the selection of the value for m is empirically determined based on the characteristics of the THz system utilized for data acquisition (TOPTICA TeraFlash Pro). Specifically, the deblurring process is conducted until the spectral bands exhibit minimal noise (in our case up to a frequency of 2 THz). The unknown blur is assumed to

be spatially invariant, but frequency-dependent. By assuming the unknown underlying image $\mathbf{x}_i$ and unknown blur $\mathbf{H}_i$, the model in equation (2) is ill-posed thus requesting regularization.

To perform blind deblurring of each band, the following optimization problem is formulated:

$$\hat{\mathbf{x}}_i, \hat{\mathbf{h}}_i = \underset{\mathbf{x}_i, \mathbf{h}_i}{\arg\min} \frac{1}{2} ||\mathbf{y}_i - \mathbf{H}\mathbf{x}_i||_2^2 + \alpha\phi(\mathbf{x}_i) + \beta\psi(\mathbf{h}_i), \quad (3)$$

where $\mathbf{h}_i$ is a vectorised form of blurring filter $\mathbf{H}_i$. The first term of the objective functions is a data fidelity term, premised on the assumption of additive white Gaussian noise. The terms ϕ and ψ act as regularizers that encode prior knowledge about the image being recovered and the blurring kernel respectively, each weighted by their respective regularization parameters, α and β.

Given that simultaneously estimating the latent image $\mathbf{x}$ and the blurring kernel $\mathbf{h}$ leads to an ill-posed optimization problem, our strategy is to first estimate the blurring kernel followed by a non-blind deconvolution to restore the image.

Kernel Estimation. Should we employ a consistent THz time-domain system and maintain identical settings for data acquisition, we can enhance the accuracy of the blurring kernel estimation by utilizing a straightforward sample, such as a circular object. This refined kernel estimate can subsequently be applied to deblur more intricate samples.

The PSF corresponding to each lower-frequency band is estimated by solving

$$\hat{\mathbf{h}}_i = \underset{\mathbf{h}_i}{\arg\min} \frac{1}{2} ||\mathbf{y}_i - \mathbf{X}_{i,j}\mathbf{h}_i||_2^2 + \beta||\mathbf{h}_i||_2^2, \quad (4)$$

where $\mathbf{X}_{i,j} \in \mathbb{R}^{bn \times bn}$ is the matrix representing the convolution of one band $\mathbf{x}_i$ and the kernel corresponding to that component, $\mathbf{h}_i$. Blurring kernel estimation from (4) is a convex optimization problem and has a closed-form solution.

To estimate the kernels, we use a simple shape object, i.e., a circular hole in a metallic surface. From this experiment, we conclude that beyond a certain frequency (e.g., 2 THz), the estimate becomes unreliable most likely due to noise.

Image Estimation. To estimate the underlying image, we solve

$$\hat{\mathbf{x}}_i = \operatorname*{argmin}_{\mathbf{x}_i} \frac{1}{2}||\mathbf{y}_i - \mathbf{H}_i\mathbf{x}_i||_2^2 + \alpha\phi(\mathbf{x}_i). \qquad (5)$$

Here, we use the regularizer formulated as a sum of two so-called l_0-norms on image intensities and gradients with the following form

$$\phi(\mathbf{x}_i) = \lambda||\mathbf{x}_i||_0 + ||\nabla\mathbf{x}_i||_0, \qquad (6)$$

with λ controlling the relative contribution of each component.

We utilize a half-quadratic splitting method for the optimization to recover the sharp image. For an indepth explanation of this approach, please refer to the work by Xu *et al.* and the citations therein (Xu et al., 2011).

Our image restoration method builds upon the framework initially presented in (Pan et al., 2014), which was specifically developed for images containing text. Furthermore, it has been demonstrated that the scope of this method extends beyond textual imagery, proving its efficacy in deblurring a broader range of natural images as well.

2.2 Low-Rank Representation

It has been demonstrated that THz HS images can be projected onto a lower dimensional subspace with almost no loss of useful information (Ljubenović et al., 2020). The number of subspace components strongly depends on the material composition of a sample and important features of the sample that should be preserved (edges, textural features, etc.). Thus, after we perform deblurring of bands corresponding to lower frequencies, we remove the remaining noise by exploiting a low-rank property of a THz HS cube.

Under the assumption that the columns of $\mathbf{X}$ in equation (1) live in a p-dimensional subspace $\mathcal{S}_p$, with $p \ll b$, spanned by the columns of subspace basis $\mathbf{E} = [\mathbf{e}_1,...,\mathbf{e}_p] \in \mathbb{R}^{b\times p}$, the underlying image is represented as $\mathbf{X} = \mathbf{EZ}$. Here, $\mathbf{Z} \in \mathbb{R}^{p\times n}$ holds the representation coefficients of $\mathbf{X}$ in $\mathcal{S}_p$. The above assumption is enabled by the discovery that $\mathbf{E}$ may be learned directly from $\mathbf{Y}$ by applying a *singular value decomposition* (SVD) or subspace identification methods such as HySime (Nascimento and Bioucas-Dias, 2007).

By projecting the original THz HS image onto a lower dimensional subspace, we remove a bulk of noise. The remaining noise can be further removed by applying a so-called plug-and-play approach and an off-the-shelf denoiser to each separate subspace component $\mathbf{z}_k$, for $k = 1, 2, ..., p$, as introduced in (Zhuang

and Bioucas-Dias, 2018). In this work, we use two off-the-shelf denoisers, namely BM3D (Dabov et al., 2007) and DnCNN (Zhang et al., 2017).

3 EXPERIMENTAL RESULTS

The results obtained by the proposed approach are compared to several state-of-the-art approaches for denoising HS images: FastHyDe (Zhuang and Bioucas-Dias, 2018), FastHyMix (Zhuang and Ng, 2023), FastSuDeep (Zhuang et al., 2021), and SSTV (Aggarwal and Majumdar, 2016). We also compared with a method for deblurring HS images, PCA + TV (Liao et al., 2013), and a method for joint THz image deblurring and denoising (Ljubenović et al., 2020).

In all experiments, the number of subspace components is set to 10, $\alpha = 0.001$, $\beta = 0.1$, and the number of iterations for kernel estimation is set to 30.

Figure 4 showcases the restoration results for the 1-cent coin using various methods. The denoising techniques for HS imagery, FastHyDe, FastHyMix, and FastSuDeep, leverage the low-rank property of HS data akin to our approach. However, these methods are originally designed for image denoising and specifically optimized for HS remote sensing imagery. In a similar vein, both the PCA + TV deblurring approach and the SSTV denoising technique are devised for remote sensing data where a uniform blurring effect across all bands is presumed. A joint deblurring and denoising method is proposed specifically for THz time-domain images where the blur removal is performed after dimensionality reduction. Due to the careful design of the proposed approach, we are able to better preserve fine details from the bands corresponding to lower frequencies and simultaneously remove noise from the higher frequency bands.

Additionally, we demonstrate the outcomes achieved on a sample possessing fine details, such as a pendant with intricate engravings (Figure 5). The results are displayed for three selected frequencies: a lower frequency (0.35 THz) predominantly affected by blurring artifacts and two higher frequencies (4 and 5.85 THz) where the original bands are heavily corrupted by strong noise.

The evaluation of our method on both the 1-cent coin and the engraved pendant samples illustrates its robustness across the entire frequency spectrum assessed. It effectively enhances the clarity of bands at lower frequencies while simultaneously reducing noise in the higher-frequency bands. It is important to note, however, that some methods we tested, such as FastHyDe, FastHyMix, FastSuDeep, and SSTV, are
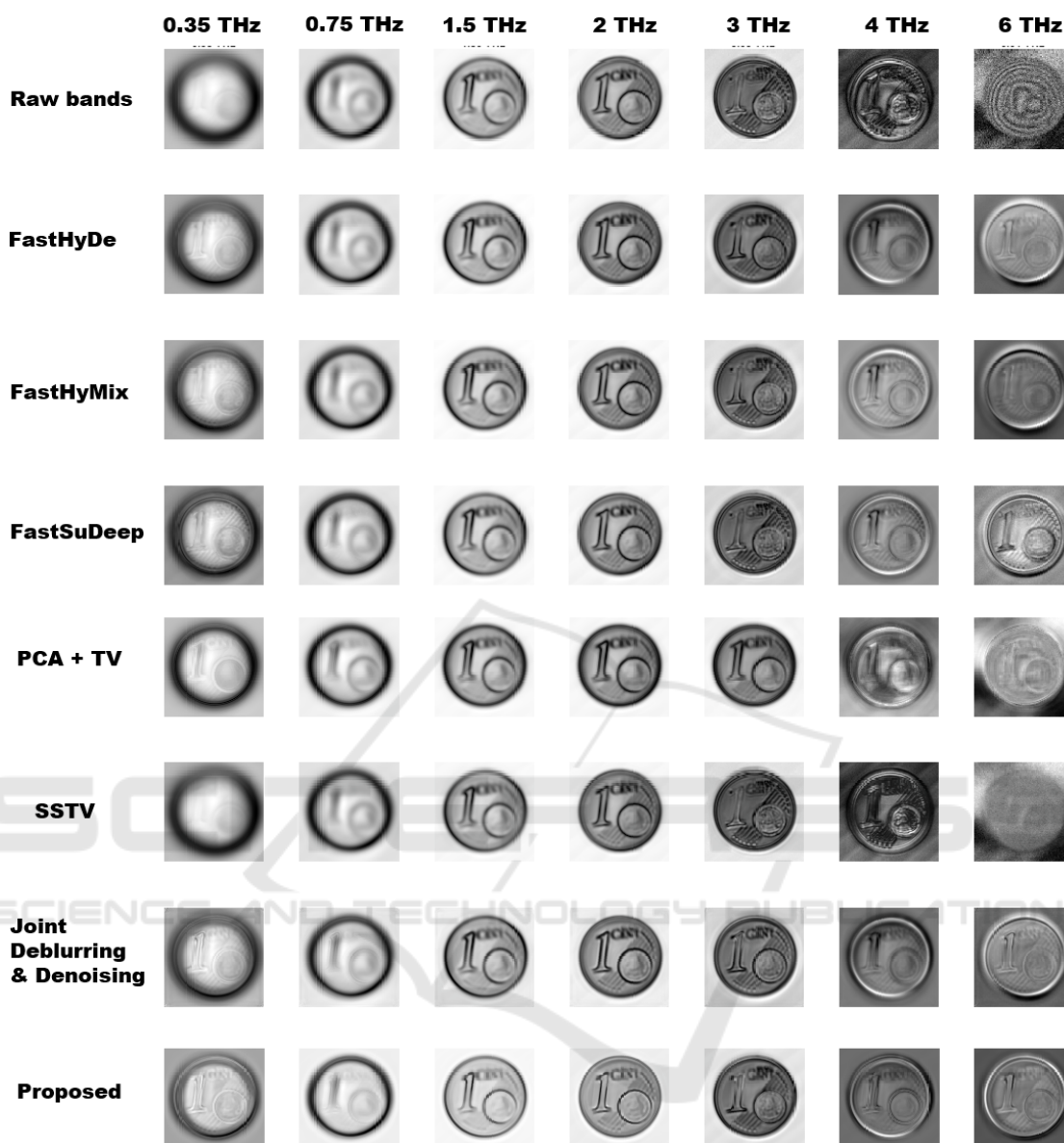
Figure 4: Results obtained on the 1 cent coin. The first row shows raw bands on seven different frequencies (from low to high). Rows two to seven show the results obtained by six different methods for denoising and deblurring of HS cubes (FastHyDe, FastHyMix, FastSuDeep, PCA + TV, SSTV, Joint Deblurring & Denoising). The final row shows the results obtained by the proposed method.

designed primarily for noise reduction and do not address the blurring present in lower-frequency bands. While PCA + TV is aimed at blur and noise removal, it falls short when confronting the strong noise levels typical in THz HS images. Although the tested joint deblurring and denoising method can mitigate both noise and blur, our proposed technique exhibits a more refined restoration of small details, particularly in lower frequencies up to 2 THz.

To compare the results of the proposed approach by using two different off-the-shelf denoisers (BM3D and DnCNN) within the plug-and-play approach explained in Subsection 2.2, we performed an experiment with the 1-cent coin (Figure 6). All other variables set in the experiments are the same. The performance of the two (plugged) denoising algorithms, BM3D and DnCNN, was found to be closely comparable. DnCNN may be given a marginal preference due to its ability to run effectively without the need for manual adjustment of input parameters.

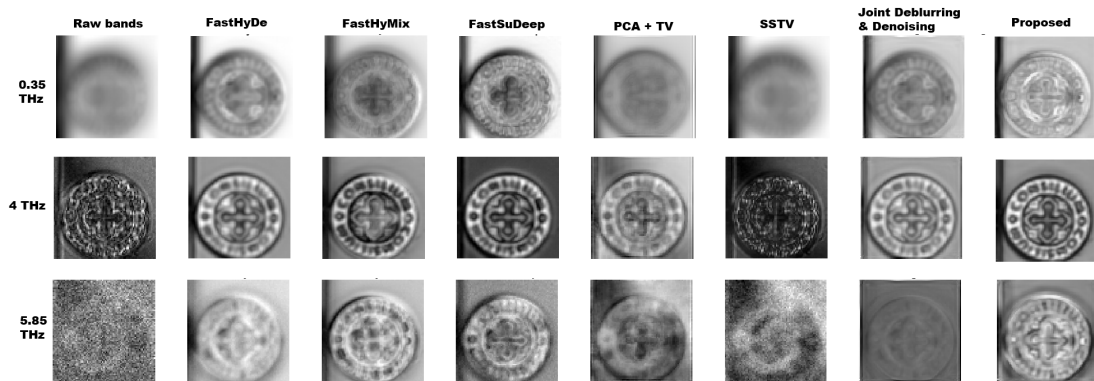To evaluate the effectiveness of our method on THz time-domain imagery that reveals layered com-

Figure 5: Results obtained on a silver pendant. The first row shows the results for the lower frequency (0.35 THz), and the middle and last rows show the results for the higher frequencies (4 THz and 5.85 THz respectively).
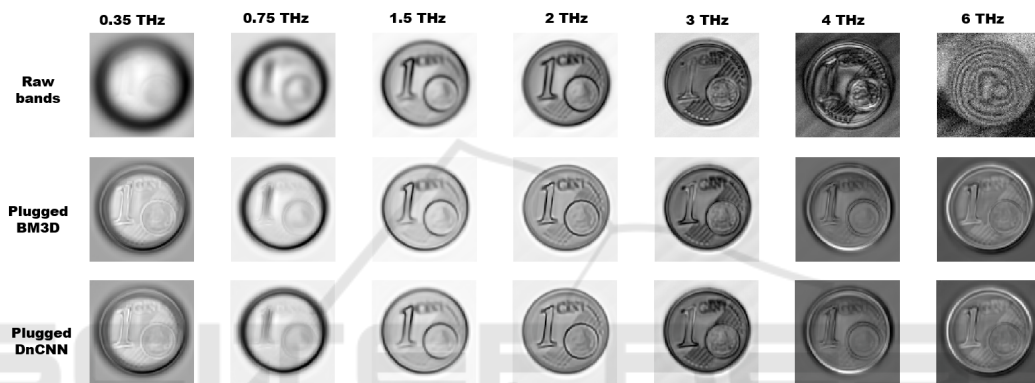

Figure 6: Results obtained with two different off-the-shelf denoisers plugged into the plug-and-play approach used for additional denoising of subspace components.
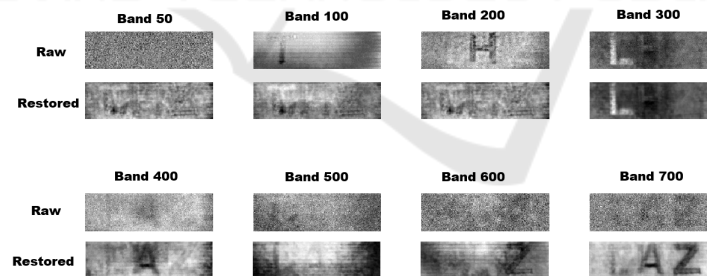

Figure 7: Results obtained with the proposed approach on a sample representing a "closed book".

positions, such as multiple layers of paper, we applied our technique to data presented in (Redo-Sanchez et al., 2016). This dataset comprises a stack of 9 pages, each imprinted with a single character (T, H, Z, L, A, B, C, C, G). Only the top page is directly observable, while the subsequent eight are concealed. The data collection was conducted using a FICO THz time-domain system from Zomega Terahertz Corporation, which has a bandwidth capability of up to 2 THz.

Figure 7 displays the results obtained with our proposed methodology on a sample referred to as the "closed book". Given that the THz scanning system utilized for data acquisition differs from our system, a minor modification to our technique is needed, including the direct estimation of PSFs for various frequency bands from the data itself. The findings confirm the resilience of our method, even when applied to datasets characterized by distinctly unique blur and noise profiles. Our approach successfully restores frequency-specific bands and unveils some of the concealed text, all without the need for any preliminary preprocessing steps. We also present selected subspace components, eigen-images, in Figure 8. No-
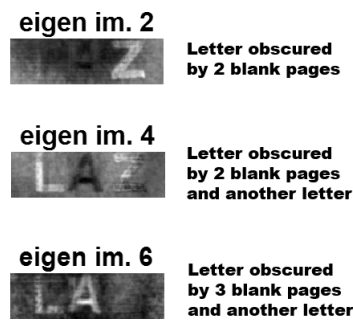
Figure 8: Selected eigen images of "closed book" showing visibility of letters obscured by blank pages and/or another leters.

tably, it is possible to discern letters from deeper layers; for instance, the letters 'L' and 'A' on the fourth and fifth pages, respectively, despite being masked by other (blank) pages and letters.

4 CONCLUSION

We introduced a new methodology for the simultaneous deblurring and denoising of THz time-domain images. Addressing the challenge of pronounced blurring at lower frequencies and significant noise at higher frequencies, we developed a two-pronged process: 1) a selective band-by-band deblurring for the lower frequency bands, and 2) a projection of the HS data cube onto a lower-dimensional subspace to effectively mitigate noise. The initial results are encouraging, demonstrating robust performance across the frequency spectrum. This is particularly noteworthy given that various samples may exhibit distinct characteristics at different frequencies within the THz range. Moving forward, our efforts are directed towards evaluating our approach on complex, multi-layered samples, including sealed ancient manuscripts, to validate further and refine our method.

ACKNOWLEDGEMENTS

REFERENCES

Aggarwal, H. K. and Majumdar, A. (2016). Hyperspectral image denoising using spatio-spectral total variation. *IEEE Geoscience and Remote Sensing Letters*, 13(3):442–446.

Candès, E. J., Li, X., Ma, Y., and Wright, J. (2011). Robust principal component analysis? *J. ACM*, 58(3).

Dabov, K., Foi, A., Katkovnik, V., and Egiazarian, K. (2007). Image Denoising by Sparse 3-D Transform-Domain Collaborative Filtering. *IEEE Transactions on Image Processing*, 16(8):2080–2095.

Darmo, J., Tamosiunas, V., Fasching, G., J.Kröll, Unterrainer, K., Beck, M., Giovannini, M., Faist, J., Kremser, C., and Debbage, P. (2004). Imaging with a Terahertz Quantum Cascade Laser. *Optics Express*, 12(9):1879–1884.

Dutta, B., Root, K., Ullmann, I., Wagner, F., Mayr, M., Seuret, M., Thies, M., Stromer, D., Christlein, V., Schür, J., Maier, A., and Huang, Y. (2022). Deep learning for terahertz image denoising in nondestructive historical document analysis. *Scientific Reports*, 12.

Fukunaga, K. (2012). Thz technology applied to cultural heritage. pages 1–4.

Hashimoto, K. and Tripathi, S. R. (2022). Non-destructive identification of drugs in plastic packaging using attenuated total reflection terahertz time domain spectroscopy. *Optics*, 3(2):99–106.

Kemp, M. C., Taday, P. F., Cole, B. E., Cluff, J. A., Fitzgerald, A. J., and Tribe, W. R. (2003). Security Applications of Terahertz Technology. In Hwu, R. J. and Woolard, D. L., editors, *Terahertz for Military and Security Applications*, volume 5070, pages 44–52.

Li, Z., Cen, Z., and Li, X. (2017). A terahertz image super-resolution reconstruction algorithm based on the deep convolutional neural network. In Jiang, Y., Gong, H., Chen, W., and Li, J., editors, *AOPC 2017: Optical Sensing and Imaging Technology and Applications*, volume 10462, pages 353 – 361. International Society for Optics and Photonics, SPIE.

Liao, W., Goossens, B., Aelterman, J., Luong, H., Pizurica, A., Wouters, N., Saeys, W., and Philips, W. (2013). Hyperspectral Image Deblurring with PCA and Total Variation. In *2013 5th Workshop on hyperspectral image and signal processing : evolution in remote sensing (WHISPERS)*, page 4. IEEE.

Ljubenović, M., Bazrafkan, S., Beenhouwer, J. D., and Sijbers, J. (2020). Cnn-based deblurring of terahertz images. In *Proceedings of the 15th International Joint Conference on Computer Vision, Imaging and Computer Graphics Theory and Applications (VISAPP)*, volume 4, pages 323–330.

Ljubenović, M., Artesani, A., Bonetti, S., and Traviglia, A. (2022). Beam-shape effects and noise removal from thz time-domain images in reflection geometry in the 0.25 - 6 thz range. *IEEE Transactions on Terahertz Science and Technology*, 12:574–586.

Ljubenović, M., Zhuang, L., De Beenhouwer, J., and Si-

jbers, J. (2020). Joint deblurring and denoising of thz time-domain images. *IEEE Access*, 9:162–176.

Long, Z., Wang, T., You, C., Yang, Z., Wang, K., and Liu, J. (2019). Terahertz image super-resolution based on a deep convolutional neural network. *Applied Optics*, 58(10):2731–2735.

Nascimento, J. M. P. and Bioucas-Dias, J. M. (2007). Hyperspectral Signal Subspace Estimation. In *IEEE International Geoscience and Remote Sensing Symposium*, pages 3225–3228.

Pan, J., Hu, Z., Su, Z., and Yang, M.-H. (2014). Deblurring text images via l0-regularized intensity and gradient prior. In *2014 IEEE Conference on Computer Vision and Pattern Recognition*, pages 2901–2908.

Podzorov, A., Wojdyla, A., and Gallot, G. (2010). Beam waist measurement for terahertz time-domain spectroscopy experiments. *Opt. Lett.*, 35(7):901–903.

Popescu, D. C. and Hellicar, A. D. (2010). Point Spread Function Estimation for a Terahertz Imaging System. *EURASIP Journal on Advances in Signal Processing*, 2010(1):575817.

Recur, B., Guillet, J. P., Manek-Hönninger, I., Delagnes, J. C., Benharbone, W., Desbarats, P., Domenger, J. P., Canioni, L., and Mounaix, P. (2012). Propagation Beam Consideration for 3D THz Computed Tomography. *Optics Express*, 20(6):5817–5829.

Redo-Sanchez, A., Heshmat, B., Aghasi, A., Naqvi, S., Zhang, M., Romberg, J., and Raskar, R. (2016). Terahertz time-gated spectral imaging for content extraction through layered structures. *Nature Communications*, 7(1).

Venkatakrishnan, S. V., Bouman, C. A., and Wohlberg, B. (2013). Plug-and-play priors for model based reconstruction. In *2013 IEEE Global Conference on Signal and Information Processing*.

Xu, L., Lu, C., Xu, Y., and Jia, J. (2011). Image smoothing via l0 gradient minimization. *ACM Trans. Graph.*, 30(6):1–12.

Zhang, K., Zuo, W., Chen, Y., Meng, D., and Zhang, L. (2017). Beyond a gaussian denoiser: Residual learning of deep cnn for image denoising. *Trans. Img. Proc.*, 26(7):3142–3155.

Zhuang, L. and Bioucas-Dias, J. M. (2018). Fast Hyperspectral Image Denoising and Inpainting Based on Low-Rank and Sparse Representations. *IEEE Journal of Selected Topics in Applied Earth Observations and Remote Sensing*, 11(3):730–742.

Zhuang, L. and Ng, M. K. (2023). Fasthymix: Fast and parameter-free hyperspectral image mixed noise removal. *IEEE Transactions on Neural Networks and Learning Systems*, 34(8):4702–4716.

Zhuang, L., Ng, M. K., and Fu, X. (2021). Hyperspectral image mixed noise removal using subspace representation and deep cnn image prior. *Remote Sensing*, 13(20).